Autophagy 9:3, 361–373; March 2013; © 2013 Landes Bioscience

Regulation of nutrient-sensitive autophagy by uncoordinated 51-like kinases 1 and 2

Fiona McAlpine,[1] Leon E. Williamson,[2] Sharon A. Tooze[1,*] and Edmond Y.W. Chan[2,*]

[1]London Research Institute; Cancer Research UK; Secretory Pathways Laboratory; London, UK; [2]Strathclyde Institute of Pharmacy and Biomedical Sciences; RICAS Group; University of Strathclyde; Glasgow, Scotland

Keywords: ULK1, ULK2, WIPI1, WIPI2, knockout, MEF, nutrient starvation

Abbreviations: ACC, acetyl-CoA carboxylase; AMPK, AMP-activated protein kinase; BafA1, bafilomycin A_1; BECN1, Beclin 1; MTOR, mechanistic target of rapamycin; PtdIns3K, phosphatidylinositol 3-kinase; PtdIns3P, phosphatidylinositol 3-phosphate; RB1CC1, RB1-inducible coiled-coil 1; RPS6, ribosomal protein S6; SQSTM1, sequestosome 1; ULK, uncoordinated 51-like kinase; ZFYVE1, zinc finger, FYVE domain-containing 1

Macroautophagy, commonly referred to as autophagy, is a protein degradation pathway that occurs constitutively in cells, but can also be induced by stressors such as nutrient starvation or protein aggregation. Autophagy has been implicated in multiple disease mechanisms including neurodegeneration and cancer, with both tumor suppressive and oncogenic roles. Uncoordinated 51-like kinase 1 (ULK1) is a critical autophagy protein near the apex of the hierarchal regulatory pathway that receives signals from the master nutrient sensors MTOR and AMP-activated protein kinase (AMPK). In mammals, ULK1 has a close homolog, ULK2, although their functional distinctions have been unclear. Here, we show that ULK1 and ULK2 both function to support autophagy activation following nutrient starvation. Increased autophagy following amino acid or glucose starvation was disrupted only upon combined loss of ULK1 and ULK2 in mouse embryonic fibroblasts. Generation of PtdIns3P and recruitment of WIPI2 or ZFYVE1/DFCP1 to the phagophore following amino acid starvation was blocked by combined *Ulk1/2* double knockout. Autophagy activation following glucose starvation did not involve recruitment of either WIPI1 or WIPI2 to forming autophagosomes. Consistent with a PtdIns3P-independent mechanism, glucose-dependent autophagy was resistant to wortmannin. Our findings support functional redundancy between ULK1 and ULK2 for nutrient-dependent activation of autophagy and furthermore highlight the differential pathways that respond to amino acid and glucose deprivation.

Introduction

Macroautophagy, henceforth referred to as autophagy, is a constitutive cellular housekeeping process, which can be induced by various stressors. A unique double-membrane organelle, the autophagosome, forms and engulfs a portion of the cytoplasm, including organelles, long-lived proteins and protein aggregates. The autophagosome then fuses with a lysosome to effect degradation of its cargo. This process is conserved from yeast to mammals, is implicated in cancer and neurodegenerative disorders, and has recently been extensively reviewed.[1-3]

ULK1, a mammalian homolog of the *C. elegans* uncoordinated 51 serine threonine protein kinase,[4,5] was first identified as a key regulator of autophagy via a kinome siRNA screen.[6] In mammals, but not lower organisms, ULK1 has a close relative, ULK2, with high homology in the kinase domain as well as the C-terminal domain.[7,8] Before being implicated in autophagy, ULK1 and ULK2 were shown to play a critical role for neuronal development.[9-11] ULK1 and ULK2 form complexes with the mammalian ortholog of yeast Atg13 and focal adhesion kinase family interacting protein of 200 kDa (RB1CC1/FIP200), the proposed mammalian functional ortholog of yeast Atg17.[7,12,13] This complex has been shown in various cell settings to be required for the activation of autophagy in combination with additional regulatory factors such as C12orf44/ATG101.[14-16] Upon amino acid withdrawal, the ULK complex translocates to the PAS (phagophore assembly site), or other sites of forming autophagosomes.[6,17,18]

ULK1/2 activity is regulated by the kinase MTOR, which forms part of the master nutrient sensor MTOR complex 1 (MTORC1). Upon amino acid starvation of cells, MTORC1 is inhibited, which releases ULK1/2 and facilitates maximal activation of the ULK-ATG13-RB1CC1 complex.[13,15] There is evidence that part of the regulation from MTORC1 involves direct phosphorylation of ULK1 which further modulates AMP-activated protein kinase (AMPK)-mediated phosphorylation of ULK1.[19-22] Interestingly, ULK1 can also inhibit MTORC1,[23] placing it both up- and downstream of the nutrient signaling cascade to provide a feedback mechanism within the system. ULK1 autophagy function can be regulated by other modifications

*Correspondence to: Sharon A. Tooze and Edmond Y.W. Chan; Email: sharon.tooze@cancer.org.uk and edmond.chan@strath.ac.uk
Submitted: 04/27/12; Revised: 11/21/12; Accepted: 11/30/12
http://dx.doi.org/10.4161/auto.23066

such as acetylation through the glycogen-synthase 3-KAT5/TIP60 pathway.[24]

Relating to physiological in vivo roles, ULK1 and ULK2 display very similar tissue expression profiles[4,5,8] although some isoform-specific functions have been described. *Ulk1*-deficient mice are born with no obvious phenotype and mouse embryonic fibroblasts (MEF) derived from these mice show normal general autophagy suggestive of ULK1/2 in vivo redundancy.[25] *Ulk2*-null mice are also born without phenotype and the corresponding MEFs show normal autophagy.[26] However, *Ulk1* knockout mice do display defects in mitochondrial autophagy during erythrocyte development and in primary hepatocytes.[25,27] Consistent with the concept of ULK1-specific in vivo roles, ULK1 was the critical isoform required for autophagy induced through low potassium-mediated membrane depolarization in primary cerebellar granule neurons.[26] In HEK293 cells, we have shown that siRNA-mediated depletion of ULK1, but not ULK2, is sufficient to inhibit autophagy which further supports how particular ULK isoforms can have predominant roles in certain cell contexts.[6]

In this study, we aimed to more definitively define roles of ULK1 and ULK2. We generated MEFs genetically targeted in both *Ulk1* and *Ulk2* and investigated their respective roles in basal and starvation-induced autophagy. To evaluate effects on autophagy, we used relatively late markers such as lipidation of LC3, the well-characterized ortholog of yeast Atg8, microtubule-associated protein 1 light chain 3 (LC3). For additional insight, we investigated earlier molecular markers of autophagy initiation by detecting membranes containing the phosphatidylinositol 3-phosphate (PtdIns3P)-binding protein WIPI2.[28] Our previous work has shown WIPI2 is found on the PAS or phagophore initiation membranes associated with the ER, where it becomes transferred to nascent autophagosomes. Here, we found that ULK1 and ULK2 are required together for autophagy induction by both amino acid and glucose withdrawal. Nutrient-dependent formation of PtdIns3P-containing autophagy membranes and LC3 lipidation are both robustly inhibited only in the combined absence of ULK1 and ULK2. Interestingly, we found that glucose starvation activates LC3 lipidation without generation of PtdIns3P, which has been previously proposed as essential for autophagy.[29]

Results

ULK1 and 2 are both required for induction of autophagy by amino acid starvation. Mice defective in essential autophagy genes *Atg5, Atg7* and *Atg9a* exhibit neonatal lethality during the post-birth starvation period.[30-32] In contrast, previously derived *Ulk1*-deficient mice are viable and fertile, with overall functional autophagy and only delayed autophagic mitochondrial clearance in reticulocytes during erythrocyte development.[25] We hypothesized that ULK1-independent autophagy was maintained in vivo through functional compensation by its closely related homolog, ULK2,[8] previously thought to have only a minor role in autophagy based on cell line work.[6] We generated *Ulk1*-deficient mice using embryonic stem cells carrying a splice acceptor gene trap within a large intronic region of the mouse *Ulk1* locus that disrupts the protein near its N terminus (details in **Fig. S1**). As expected, homozygous *Ulk1* gene trap knockout mice (ULK1KO) were viable, fertile and showed no differences from wild-type (WT) in growth or survival. *Ulk2*-deficient mice have also been shown to be viable, fertile and capable of autophagy.[26] We derived MEFs from ULK1KO, ULK2KO and WT embryos and analyzed autophagy properties in primary and SV40 T antigen immortalized sublines. Immortalized ULK1KO MEFs showed reduced ability to regulate amino acid starvation-induced autophagy as assessed by LC3 lipidation (**Fig. 1A**) (serum was also absent during short-term amino-acid starvation). ULK1KO MEFs had significantly lower LC3-II/LC3-I ratios under both full-nutrient and amino acid-starved conditions as compared with WT MEFs, although ULK1KO cells displayed some residual ability to increase LC3-II in response to amino acid starvation. In contrast, ULK2KO MEFs displayed an alternate phenotype of abnormally elevated LC3-II/LC3-I under both full-nutrient and amino acid-starved conditions. Lipidation of LC3 was further measured following amino acid starvation in the presence of the vacuolar proton ATPase inhibitor bafilomycin A_1 (BafA1) to assess autophagic flux when lysosomal function was inhibited. WT MEFs show robust LC3-II accumulation under amino acid starvation + BafA1 conditions as expected. Consistent with effects under amino acid starvation, ULK1KO MEFs showed approximately 50% decreased LC3-II accumulation following starvation + BafA1. Conversely, ULK2KO MEFs

Figure 1 (See opposite page). Loss of ULK1 and ULK2 inhibits autophagy following amino acid starvation. (**A**) Wild-type (WT), *Ulk1* knockout (ULK1KO), *Ulk2* knockout (ULK2KO) and two independently derived *Ulk1/Ulk2* double knockout (DKO) MEF lines were treated with full-nutrient medium (F), EBSS (–AA) or EBSS containing 50 nM bafilomycin A_1 (Baf) for 2 h. Resolved cell lysates were immunoblotted with antibodies against ULK1, actin and LC3 (Nanotools 5F10 monoclonal). "*" indicates nonspecific band on ULK1 immunoblot. MEF lines were immortalized with SV40 T antigen. Below: LC3-II/LC3-I signals were plotted as average ± SEM, (n = 4) using 2 different y-axis scales. Two-tailed paired t-tests were performed relative to values of WT MEFs under the same condition: *p < 0.04; **p < 0.005; [a]p = 0.14; [b]p = 0.056; [c]p = 0.12. (**B**) Total RNA was extracted from MEF lines described in (**A**) and analyzed for *Ulk1* and *Ulk2* transcript levels using quantitative RT-PCR. Plots show *Ulk1* or *Ulk2* levels normalized to *Actin* transcript levels (average ± SEM, (n = 3), values relative to WT cells). (**C**) WT and DKO MEF lines were treated as in (**A**) to full-nutrient medium or EBSS for 2 h. Resolved cell lysates were immunoblotted with antibodies against phospho-(Ser79) acetyl CoA carboxylase (P-ACC), phospho-(Ser240/244) ribosomal protein S6 (P-RPS6); actin and LC3 (5F10 monoclonal antibody). (**D**) MEF lines were treated to full-nutrient medium (F) or glucose starvation (–Glc) for 16 h before lysis and immunoblot analysis as in (**C**). (**E**) MEF lines were steady-state labeled overnight with C14-valine, chased for 24 h, and analyzed for protein degradation over 2 h of amino acid starvation. Plot shows average ± SEM (n = 3). Two-tailed paired t-tests were performed relative to WT MEFs: *p < 0.02; **p < 0.01. (**F**) WT and *Ulk* DKO#1 MEFs were treated as in (**A**) for 2 h and fixed for LC3 immunostaining. Shown are representative confocal images of –AA and –AA+Baf conditions. Scale bar: 10 μm. Plots show average puncta/cell ± SEM (each column: n = 22 to 39 cells per condition from two experiments). Two-tailed paired t-tests when compared with WT MEFs under the same condition: ***p < 0.0003; *p < 0.02. (**G**) Primary WT and DKO MEFs were subjected to starvation conditions as in (**A**) and lysed for immunoblot analysis of SQSTM1 and actin. Right: Plotted densitometry [SQSTM1 levels normalized to actin, shown as average ± SEM (n = 4)]. Two-tailed paired t-tests when compared with WT MEFs under same conditions: *p < 0.04, **p < 0.01.

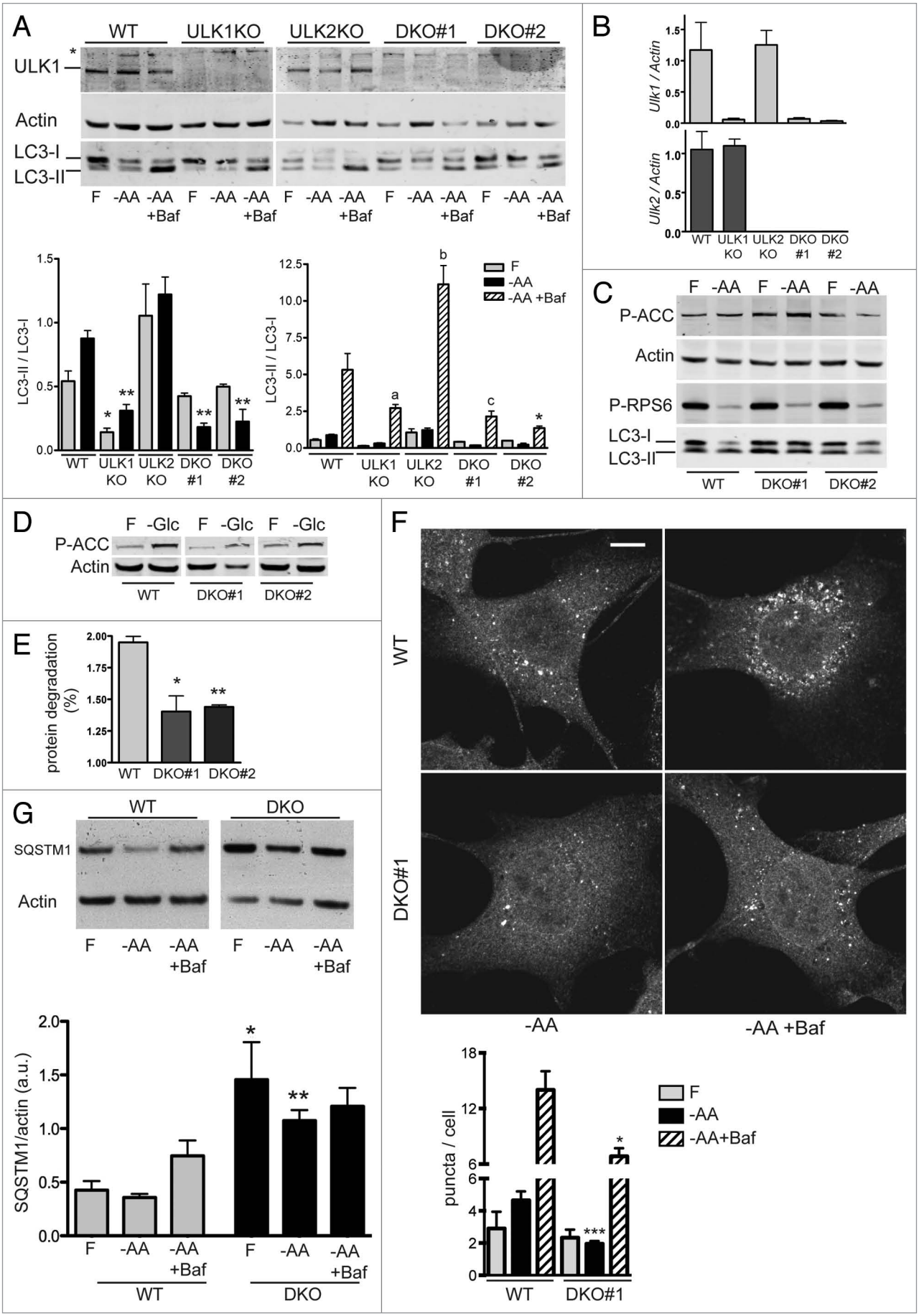
A
WT
ULK1KO
ULK2KO
DKO#1
DKO#2
ULK1
Actin
LC3-I
LC3-II
F -AA -AA +Baf
LC3-II / LC3-I
WT ULK1 KO ULK2 KO DKO #1 DKO #2
F
-AA
-AA +Baf
B
Ulk1 / Actin
Ulk2 / Actin
C
P-ACC
Actin
P-RPS6
LC3-I
LC3-II
F -Glc
D
E
protein degradation (%)
WT DKO#1 DKO#2
F
G
SQSTM1
Actin
SQSTM1/actin (a.u.)
DKO
-AA +Baf
WT
DKO#1
puncta / cell
©2013 Landes Bioscience. Do not distribute.

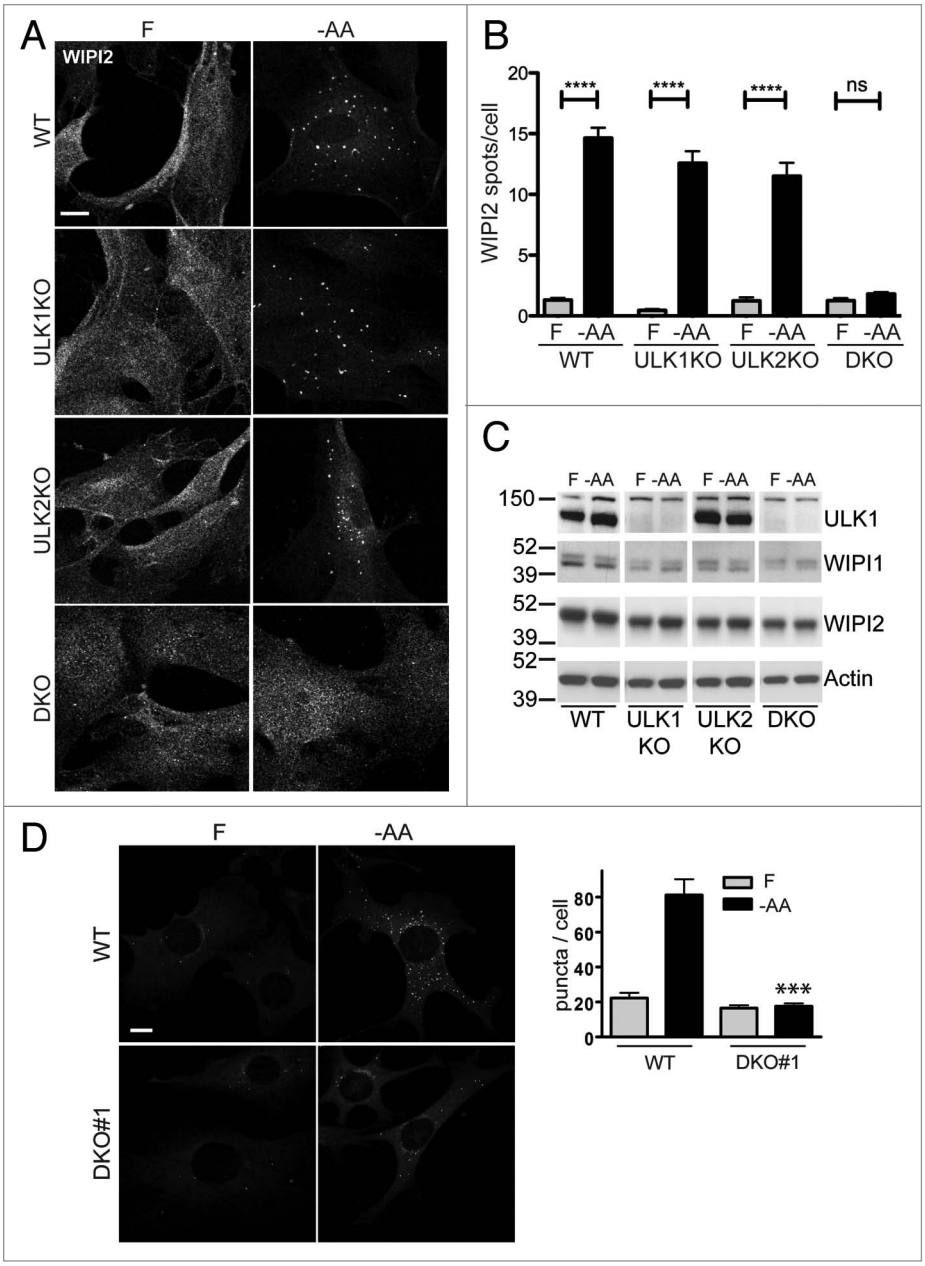

Figure 2. ULK1 and ULK2 are both required for WIPI2 spot formation following amino acid starvation. (**A**) WT, ULK1KO, ULK2KO and DKO primary MEFs were treated with either full nutrient-medium (F) or EBSS (–AA) for 2 h before fixation. Cells were then stained with an antibody against WIPI2. (**B**) In 10 fields per condition (two independent experiments) Hoechst-stained nuclei (cell number) and WIPI2 puncta were quantified (WIPI2 puncta/cell ± SEM) (n = 20 fields). Differences between F and –AA are indicated by ****p < 0.0001 by one-way ANOVA with Bonferroni post hoc test, n.s. non-significant. (**C**) Primary MEF lines were treated as in (**A**). Cell lysates were immunoblotted for ULK1, WIPI1, WIPI2 and actin. (**D**) WT and DKO#1 immortalized cells stably expressing GFP-ZFYVE1 were treated to full-nutrient medium (F) or EBSS (–AA) for 2 h before fixation. (**A and D**) Scale bars: 10 μm. Plot shows puncta/cell (average ± SEM for n = 29 to 37 cells per condition from two experiments). Two-tailed paired t-test comparing to WT MEFs under same conditions: ***p < 0.0001.

showed elevated LC3-II accumulation when cells were starved while blocking lysosomal activity. These data suggest partially disrupted amino acid-dependent autophagy in ULK1KO cells but an alternate cellular phenotype following *Ulk2* knockout that may involve compensatory mechanisms that lead to moderately elevated autophagy.

Given the functional compensation observed in mouse viability following single *Ulk1* or *Ulk2* knockout, we investigated *Ulk1/2* double-deficiency. We interbred ULK1KO and ULK2KO mice and derived MEFs from DKO embryos collected at day E13 of development. DKO MEFs showed more dramatic impairment of autophagy, with decreased LC3-II/LC3-I following amino acid starvation (as observed in 2 independent DKO MEF cell lines). Both DKO MEF lines also showed significantly decreased LC3-II accumulation following starvation + BafA1 conditions. Analysis of LC3/actin levels further confirmed the inhibition of LC3-II accumulation in DKO MEFs treated to amino acid starvation in the presence of BafA1 (**Fig. S2A**). We also confirmed in primary MEFs that *Ulk* DKO showed the clearest impairment of amino acid-dependent LC3 lipidation (**Fig. S2B**). Taken together, these results are consistent with a partial block in amino acid starvation- dependent autophagy following *Ulk1* loss, with more complete ablation following combined loss of *Ulk1* and *Ulk2*. Of note, detectable levels of autophagy (LC3 lipidation) are still observed following single or double loss of *Ulk1/2* members, in contrast with effects following *Atg5* knockout as observed in control experiments (**Fig. S2B and S2C**). As further control, we confirmed proper targeting of *Ulk1* and *Ulk2* mRNAs in these MEF lines (**Fig. 1B**).

As starvation-dependent autophagy was strongly affected following *Ulk* DKO, we investigated if amino acid signaling mechanisms to MTORC1 had been disrupted. Following amino acid starvation, MTORC1 was robustly inactivated, as expected, using levels of phosphorylated ribosomal protein RPS6 as a marker (**Fig. 1C**). MTORC1 inactivation following amino acid starvation was similar in both DKO lines. The 2 h of amino acid starvation did not activate the AMPK pathway (using phosphorylation of acetyl-CoA carboxylase (ACC) as a marker). As we used glucose starvation as a means to activate autophagy in later parts of this study, we also analyzed AMPK activation when cells were subjected to glucose-depleted conditions (**Fig. 1D**). WT MEFs displayed a 3.35-fold (± 1.8 SEM, n = 3) increase

in ACC phosphorylation (phospho-ACC/actin, normalized to the full-nutrient condition) following glucose starvation. ACC phosphorylation was also stimulated in *Ulk* DKO MEFs following glucose starvation but to a lesser extent (e.g., 1.6-fold (± 0.8 SEM, n = 3) in DKO line #2). Prolonged glucose starvation did not lead to MTORC1 inactivation in any of the cell types (**Fig. S2D**). These data suggest that amino acid deprivation leads to expected MTORC1 inactivation responses even under *Ulk* DKO cellular contexts. Furthermore, prolonged glucose starvation could activate AMPK in *Ulk* DKO cells, although this response was partially impaired.

We investigated levels of impairment in *Ulk* DKO cells using additional autophagy assays. Levels of long-term protein degradation in radiolabeled cells, a classical biochemical method of quantifying autophagic degradation, was impaired by approximately 50% in both DKO MEF lines as compared with WT cells (**Fig. 1E**). We also characterized formation of autophagic structures in WT and DKO MEFs using LC3 puncta formation (**Fig. 1F**). Amino acid starvation increased the numbers of quantified LC3-positive structures in WT MEFs. Numbers and sizes of structures were further sharply increased upon addition of BafA1 into the starvation medium. Amino-acid starvation did not stimulate formation of LC3-positive membranes in DKO cells. Accumulation of LC3-positive membranes following starvation in the presence of BafA1 was also significantly lower in DKO as compared with wild-type MEFs. As a further approach to assess autophagy capacities, we measured steady-state levels of the SQSTM1/p62 autophagy adaptor protein (**Fig. 1G**). Amino acid starvation increased SQSTM1 degradation in WT cells as expected, and inclusion of BafA1 during amino-acid starvation prevented SQSTM1 degradation. Under both amino acid replete and depleted conditions, *Ulk* DKO cells showed a general accumulation of SQSTM1 relative to WT cells, which further suggests that overall autophagic SQSTM1 degradation was impaired.

Since LC3 lipidation is a comparatively late event in autophagy,[18] we examined whether the loss of ULK1 and ULK2 affected earlier markers of autophagosome formation such as WIPI2. By functioning as a PtdIns3P effector protein, WIPI2 localizes to early phagophore structures and WIPI2 puncta formation can monitor activity of the BECN1-class III phosphatidylinositol 3-kinase (PtdIns3K) pathway.[28] Resting MEFs maintained under full nutrients do not show any detectable WIPI2-positive punctate structures. When starved of amino acids, ULK1KO and ULK2KO cells were still capable of forming WIPI2-positive puncta. However, *Ulk* DKO cells were completely blocked in this pathway (**Fig. 2A and B**). These results show that recruitment of WIPI2 during the autophagic response to amino acid starvation is dependent on both ULK1 and ULK2, as could be inferred by the position given to WIPI1 through the hierarchal analysis of autophagy regulation in MEFs.[18] Although WIPI2-positive structures are not formed in *Ulk* DKO cells, we could confirm that WIPI2 (and its related family member WIPI1) were similarly expressed in all MEF types irrespective of ULK1/2 expression (**Fig. 2C**). As an alternate strategy, we studied MEF lines stably expressing GFP-tagged zinc finger, FYVE domain containing 1/double-FYVE containing protein 1 (ZFYVE1/DFCP1) which serves as a marker for PtdIns3P-associated omegasome membranes formed upon autophagy activation (**Fig. 2D**).[33] Amino-acid starvation promoted a 4-fold increase in formation of GFP-ZFYVE1-positive membranes in WT MEFs. By contrast, DKO MEFs show only low numbers of basal GFP-ZFYVE1-positive structures but formation of these are not stimulated by amino acid starvation. These data suggest that amino acid-dependent formation of PtdIns3P-containing autophagy membranes is markedly impaired upon *Ulk1/2* DKO.

Amino acid response in ATG13-deficient cells is similar to DKO cells. In mammalian cells, ATG13 is an obligate binding partner of ULK1/2 and forms an essential part of the ULK1-containing autophagy induction complex, together with RB1CC1 and C12orf44.[7,13-16] ATG13 binds the C-terminal domain of both ULK1 and ULK2 and can be phosphorylated by these kinases.[7] Since ATG13 is essential for autophagy and can form a complex with both ULK1 and ULK2, we reasoned that ATG13 depletion should have a similar effect as the combined loss of both ULK1 and ULK2. We depleted *Atg13* in WT and DKO MEFs using siRNAs and further subjected cells to amino acid starvation (**Fig. 3**). While ATG13 showed similar steady-state expression levels in WT and DKO MEFs, ATG13 levels were clearly reduced by transient siRNA transfections. ATG13 knockdown inhibited the ability of amino acid starvation to promote LC3 lipidation in WT cells. As expected, *Ulk* DKO MEFs (treated with control siRNA) already showed impaired amino acid starvation-induced LC3 lipidation and lower amounts of LC3-II accumulation when starved in the presence of BafA1. Further ATG13 knockdown in DKO MEFs did not produce higher levels of inhibition.

To further compare effects of ATG13 depletion with *Ulk* DKO, we examined the formation of WIPI2 puncta in response to amino acid withdrawal. In agreement with LC3 data, ATG13 knockdown suppressed starvation-induced WIPI2 puncta formation in WT, *Ulk1* and *Ulk2* KO cells. *Ulk* DKO MEFs did not show amino acid starvation-induced WIPI2 puncta and ATG13 depletion had no further effect (**Fig. 4**). Control experiments confirmed that siRNA treatments did not affect WIPI2 levels in the different MEF lines (**Fig. S3**). Taken together, these data show that ATG13 depletion and *Ulk* DKO have similar inhibitory effects on amino acid withdrawal-induced autophagy. As ATG13 knockdown produced no further detectable effect within the *Ulk* DKO context, our data suggest that ATG13 primarily functions in autophagy by regulating the ULK1/2 complex.

Autophagy following glucose starvation is dependent upon ULK1/2 but not PtdIns3P. In addition to amino acid-dependent regulation, autophagy is induced when cells are starved of glucose via pathways that involve AMPK activation and increased production of the metabolic intermediate ammonia.[21,34,35] We set out to determine whether the ULK1/2 complex regulates autophagy following prolonged glucose withdrawal. WT displayed increased levels of lipidated LC3-II (normalized to actin) in response to glucose starvation (**Fig. 5**). In contrast, glucose starvation did not stimulate LC3 lipidation in DKO MEFs. As expected, high amounts of LC3-II accumulated when BafA1 was included during this prolonged period of glucose starvation and this effect was similarly robust in both WT and DKO MEFs.

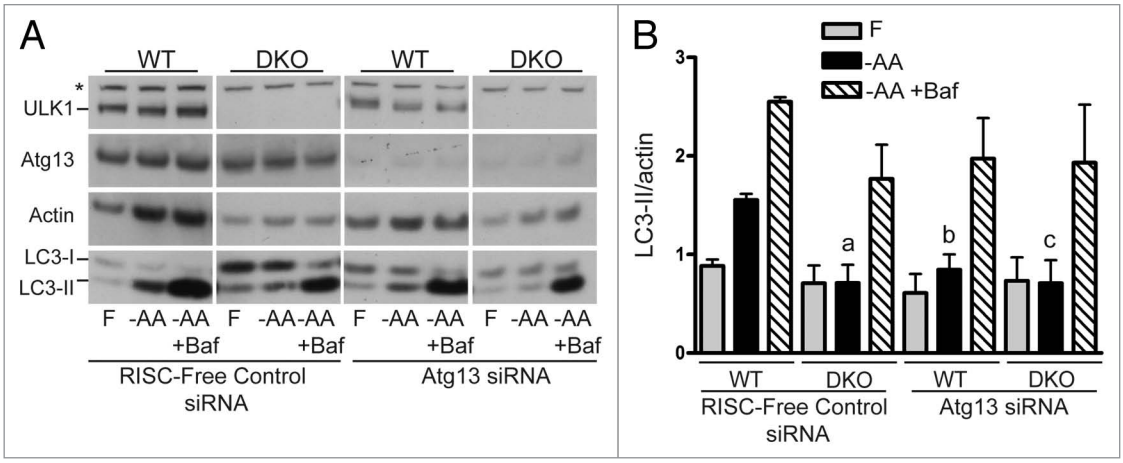

Figure 3. ATG13 knockdown phenocopies *Ulk1/Ulk2* double knockout for the LC3 lipidation pathway following amino acid starvation. (**A**) WT and DKO primary MEFs were transfected with either RISC-Free control or mouse *Atg13*-targeting siRNA. Following knockdown, cells were treated with either full-nutrient medium (F), EBSS (–AA) or EBSS containing bafilomycin A_1 (–AA+Baf) (100 nM) for 2 h. Resolved cell lysates were immunoblotted with antibodies against ULK1, ATG13, actin and LC3 (Abcam polyclonal). (**B**) Average LC3-II/actin densitometry ± SEM (n = 4). Two-tailed paired t-tests were performed relative to WT-RISC-Free siRNA MEFs under the same conditions: [a]p = 0.067; [b]p = 0.068; [c]p = 0.089.

To validate the lack of an induction of LC3-lipidation after glucose withdrawal we assayed for WIPI2 puncta formation. Surprisingly, WIPI2-localized structures failed to clearly form in glucose-starved WT MEFs (**Fig. 6**). MEFs with single or double *Ulk* knockout similarly did not show WIPI2-positive puncta following glucose starvation. From these data, we hypothesized that glucose-induced autophagy is not strictly dependent on robust accumulation of PtdIns3P, a lipid signal previously thought to be essential for autophagy.[29] To investigate this notion, we tested effects of the PtdIns3K inhibitor wortmannin on amino acid- and glucose-dependent autophagy. As expected, wortmannin significantly inhibited induction of LC3 lipidation in WT MEF following amino acid starvation down to basal levels observed in fully fed cells (**Fig. 7A**). In contrast, addition of wortmannin during glucose starvation mildly increased LC3 lipidation.

To further define roles of PtdIns3P during nutrient-dependent autophagy, we studied effects of PtdIns3K inhibition on autophagosome membrane formation. Prolonged glucose starvation stimulated the formation of LC3-labeled autophagosomes in wild-type MEFs (**Fig. 7B**). LC3-positive structures formed following glucose starvation were generally larger than those found following amino acid starvation. PtdIns3K inhibition by wortmannin produced a stronger inhibition of amino acid starvation-dependent autophagy structures. After amino acid starvation, 36% of cells showed 15 or more puncta per cell, which was reduced to 5% of cells when wortmannin was added during starvation. By comparison, after glucose starvation 24% of cells showed 15 or more puncta per cell and 15% of cells still showed 15 or more puncta per cell when wortmannin was included during glucose starvation. These findings further support the notion that glucose starvation induces a previously uncharacterized LC3 lipidation pathway that can function independently of PtdIns3P generation.

WIPI1, the close homolog of WIPI2,[28] tagged with GFP has been used as a marker for PtdIns3P-containing early autophagosomal membranes.[18,36] We have shown in cell lines that contain both WIPI1 and WIPI2, for example G361 cells, there is a substantial overlap of the endogenous proteins.[28] To further investigate the absence of WIPI2-localized membranes following glucose-starvation in WT MEFs, we compared the localization of endogenous WIPI1 and WIPI2 following amino acid or glucose starvation with and without wortmannin (**Fig. 8**). WIPI1 and WIPI2 levels were unaffected by glucose starvation with and without wortmannin (**Fig. S4**). As expected, WIPI1 and WIPI2 puncta formed following amino acid starvation of MEFs with close, but not identical, staining patterns. Formation of both WIPI1- and WIPI2-labeled structures following amino acid starvation were inhibited by wortmannin. Consistent with the above result using WIPI2 (**Fig. 6**), prolonged glucose starvation did not stimulate production of membranes containing WIPI1 or WIPI2. These unexpected findings serve to further confirm the absence of PtdIns3P generation when autophagy is activated in MEFs deprived of glucose.

Discussion

Functional redundancy of Ulk1 and Ulk2. The mammalian ULK family is the ortholog of the yeast kinase Atg1, which was the first protein identified to be required for autophagy in *S. cerevisiae*.[37] ULK proteins have since been established to play a critical role in the autophagy regulatory pathway.[38] Under the current consensus, family members such as ULK1 and ULK2 form a core autophagy regulatory complex along with ATG13, RB1CC1 and C12orf44. This core ULK complex has been proposed to integrate nutrient-dependent signals from MTORC1 and AMPK to regulate the activation of autophagy.

The mammalian ULK family contains up to five members (ULK1–4 and STK36) although only ULK1 and ULK2 show extensive sequence homology along the entire protein length.[39] The clearest evidence for ULK1/2 functional in vivo redundancy

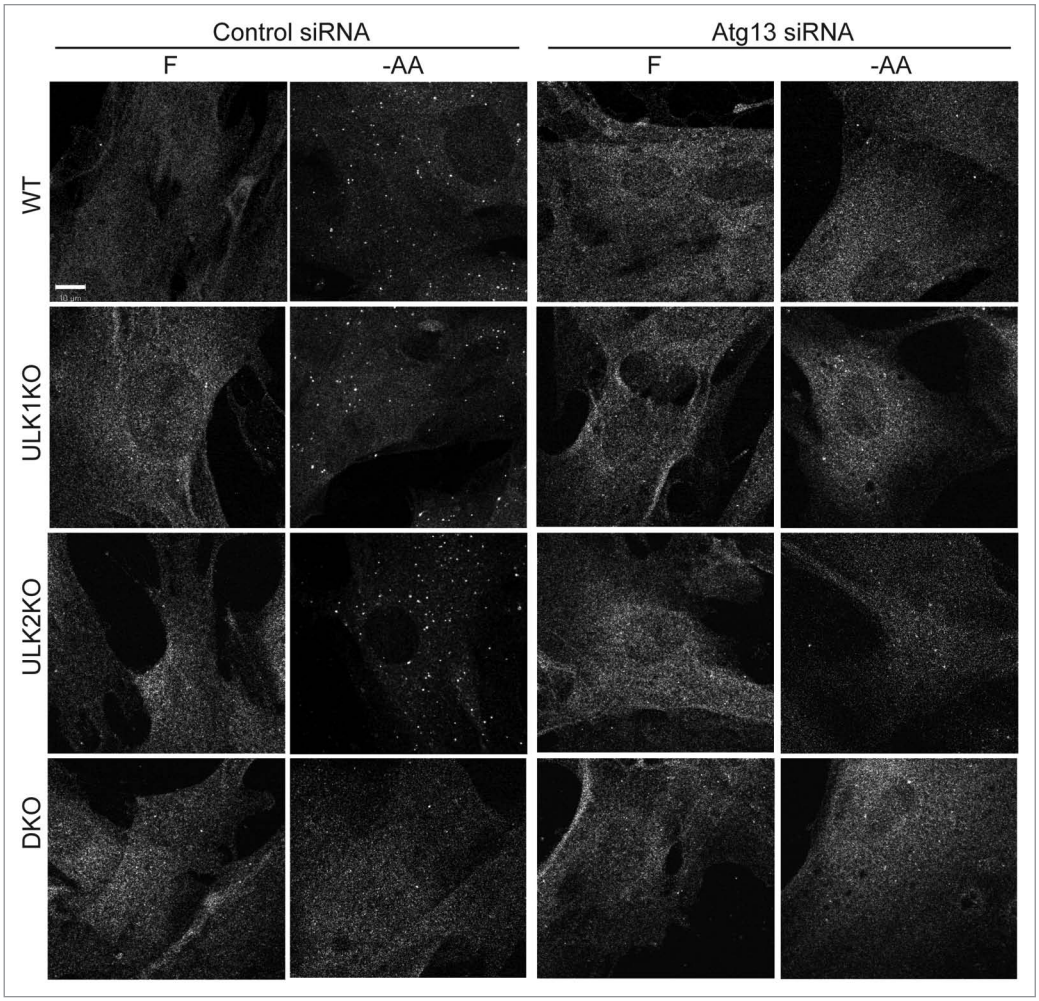

Figure 4. ATG13 knockdown phenocopies *Ulk1/Ulk2* double knockout on the formation of WIPI2-positive autophagosomal membranes following amino acid starvation. WT, ULK1KO, ULK2KO and DKO primary MEFs were transfected with either RISC-Free control or mouse *Atg13*-targeting siRNA. Following knockdown, cells were treated with either full-nutrient medium (F) or EBSS (–AA) for 2 h before fixation. Cells were stained with an antibody against WIPI2. Scale bar: 10 μm.

has been the normal mouse viability of single *Ulk1* or *Ulk2* knockout mice, which contrasts with the overt neonatal or postnatal lethality from knockout of other essential autophagy genes.[25,26,30-32] When we crossed *Ulk1* and *Ulk2* KO mouse lines to generate the *Ulk1/2* DKO model, we observed a reduction in double knockout embryos at day 13.5 and perinatal lethality (Tooze SA, unpublished).[34] Our data on the corresponding *Ulk*-deficient MEF cultures shed more light on ULK1/2 cellular functional redundancy. Loss of ULK1 resulted in a partial block of autophagy that was still nutrient-responsive. On the other hand, loss of ULK2 led to moderately elevated cellular markers of autophagy, which likely reflects compensation from ULK1. Importantly, autophagy activation by amino acid or glucose starvation was robustly inhibited when both *Ulk1* and Ulk2 are deleted. However, some residual autophagy occurs even under ULK1/2-deficiency. *Ulk1/2* DKO MEFs under nutrient starvation while lysosomal flux was blocked still accumulated lipidated LC3 and autophagosomal membranes although to a much reduced extent. These data suggest that downstream autophagy machinery still function at low but detectable rates despite absence of the ULK1/2 complex. Other published results support

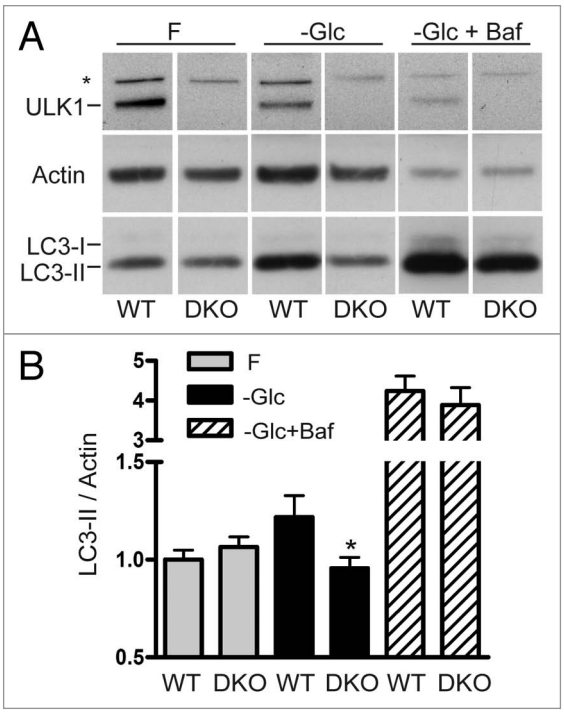

Figure 5. Combined *Ulk1* and *Ulk2* knockout reduces the LC3 lipidation response to glucose starvation. (**A**) WT or DKO primary MEFs were treated to either full-nutrient medium (F), glucose-free conditions (–Glc), or glucose-free medium + bafilomycin A_1 (–Glc+Baf) (100 nM) for 24 h. Resolved cell lysates were immunoblotted with antibodies against ULK1, actin and LC3 (Abcam polyclonal). "*" indicates nonspecific band. (**B**) LC3-II and actin signals were quantified by densitometry. Results are shown as average ± SEM (n = 4). Two-tailed paired t-tests were performed relative to WT MEFs under the same treatment: *p < 0.02.

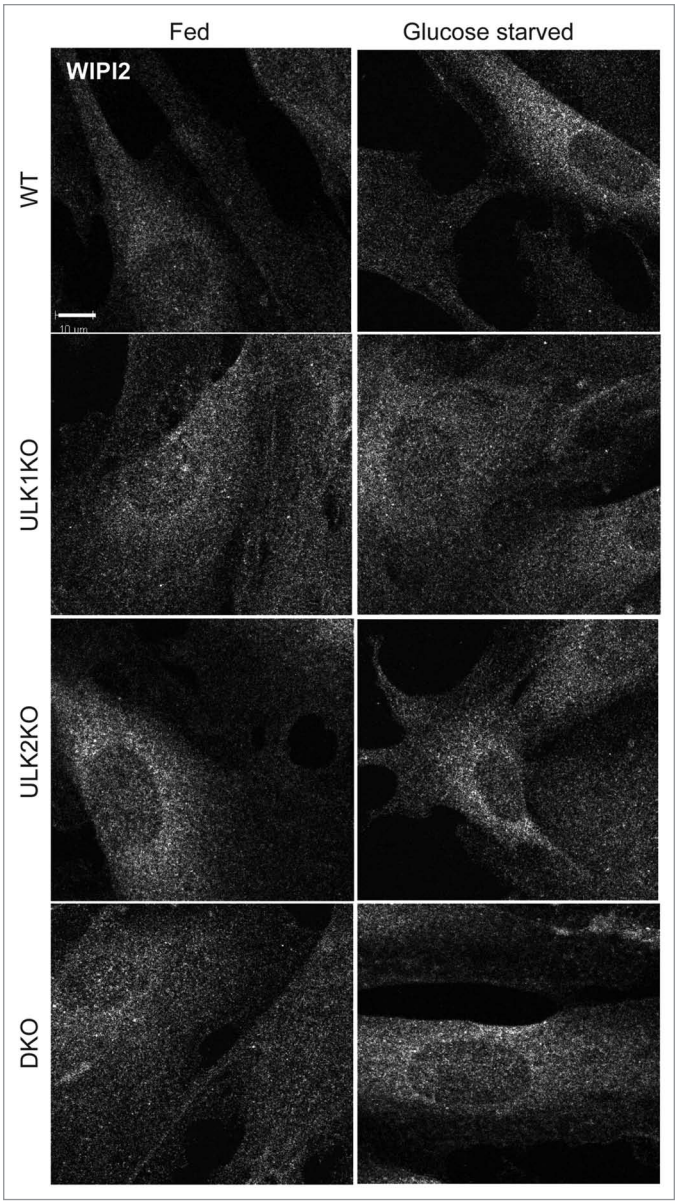

Figure 6. Glucose starvation does not stimulate production of WIPI2-containing membranes. WT, ULK1KO, ULK2KO and DKO primary MEFs were treated with either full-nutrient medium (Fed) or glucose-free medium (glucose starved) for 24 h then fixed. Cells were stained with an antibody against WIPI2. Scale bar: 10 μm.

a cellular ammonia-dependent form of autophagy that functions independently of ULK1/2.[34] It also remains possible that under *Ulk1/2* DKO conditions, other ULK family members (ULK3, ULK4 and STK36) may compensate to support low levels of residual or non-canonical autophagy. ULK3 has been implicated in a specific subtype of autophagy activated during oncogene-induced cellular senescence,[40] but neither ULK4 nor STK36 have yet been implicated in autophagy.

Our previous work has shown that ULK1/2 C-terminal domains are capable of inhibiting starvation-induced autophagy in a dominant-negative fashion[7] suggesting that these over-expressed fragments compete for necessary ULK1/2 binding partners such as ATG13 or RB1CC1.[12-14] Consistent with the concept of a critical ULK1/2-ATG13-RB1CC1 autophagy complex, we observed that ATG13 knockdown alone inhibited starvation-dependent autophagy to a similar extent as *Ulk1/2* DKO. Furthermore, ATG13 knockdown had no effect within a *Ulk1/2* DKO background, presumably as the complex was already disrupted. Our data from MEFs contrast with observations from a chicken B cell system, which suggested autophagy regulatory roles of ATG13 and RB1CC1 that were independent of ULK1/2.[41] Further studies should clarify if mammalian ATG13 and RB1CC1 have similar ULK-independent roles for autophagy in particular cellular contexts.

Glucose-starvation dependent autophagy is independent of PtdIns3P. Our further results indicate an ability of glucose-starved cells to perform autophagy in the absence of robust PtdIns3P generation, which has long been considered an obligate requirement for autophagy.[29] Early in the autophagic pathway, PtdIns3P is generated from the ER-localized PIK3C3/Vps34-BECN1-ATG14 PtdIns3K complex.[42,43] Hierarchal analysis of autophagy regulation in MEFs has positioned ULK signaling to function upstream of the PIK3C3-BECN1-ATG14 PtdIns3K complex[18] and our results using the WIPI2 and ZFYVE1 markers in *Ulk1/2* DKO MEFs are consistent with this model. As the PIK3C3-BECN1-ATG14 PtdIns3K complex translocates onto the ER, WIPI2 is recruited to PtdIns3P at the omegasome and proceeds to decorate the phagophore or nascent autophagosome. There are several reports on colocalization of WIPI and ULK family members on forming autophagosomes.[18,44] WIPI2 is required for LC3 lipidation following amino acid starvation highlighting how this role as PtdIns3P effector is required for further downstream steps of the autophagy initiation cascade.[28]

Here, we observed that cells starved of glucose fail to form WIPI2 puncta, while they do show elevated LC3 lipidation. We verified that WIPI1, the close ortholog of WIPI2,[18,36] also failed to form puncta when cells were glucose starved in agreement with Pfisterer et al. who studied the GFP-WIPI1 marker in a MEF system.[44] As both WIPI1 and WIPI2 bind PtdIns3P,[28,36] we questioned whether glucose-starved cells were capable of autophagy in the absence of PtdIns3P generation. When cells are starved of glucose, the requirement for the generation of PtdIns3P at the ER appears to be abrogated, as we detected LC3 lipidation and generation of autophagosomes even in the presence of the PtdIns3K inhibitor wortmannin. Wortmannin inhibited LC3 lipidation and membrane formation in amino acid starved cells in accordance with previous results.[29]

Autophagy pathways with differential dependence on core regulatory factors have been identified and collectively termed non-canonical autophagy.[35] An ATG5-ATG7-independent autophagy mechanism has been described[45] although loss of either of these genes presents neonatal lethality in mice.[30,31] As another example, resveratrol induces a noncanonical form of autophagy that has been shown to be BECN1 and PtdIns3P independent under certain contexts.[46] Others have reported that resveratrol-dependent autophagy was partially sensitive to wortmannin and WIPI1/2 function but occurred in the absence of WIPI1/2-positive structure formation.[47] Our own previous data from HEK293 cells has

shown reservatrol treatment to induce endogenous WIPI2-positive puncta.[28] Our data presented here suggest the possibility of glucose starvation-dependent autophagy without overt PtdIns3P generation or the recruitment of WIPI2 to the omegasome and nascent autophagosome. This pathway still required both ULK1 and ULK2, but the apparent bypass of PIK3C3-BECN1-ATG14 PtdIns3K complex during noncanonical autophagy remains to be explored.

Materials and Methods

Reagents and antibodies. Bafilomycin A_1 and wortmannin were from Calbiochem or Tocris Bioscience. SiGENOME siRNAs were produced by Dharmacon/ThermoScientific. Complete protease inhibitor tablets (04693124001) were purchased from Roche. Immobilon-P PVDF membranes (IPVH00010) were from Millipore. Amersham ECL western blotting detection reagents (RPN2106) and Amersham Hyperfilm MP high performance autoradiography film (28-9068-45) were obtained from GE Healthcare. Restore PLUS western blot stripping buffer (46430) was from ThermoScientific.

Rabbit anti-LC3B (ab48394) and rabbit anti-actin (ab8227) were from Abcam. Mouse anti-LC3 (5F10) was from Nanotools, Teningen, Germany. Mouse anti-actin (clone AC-40, all actin isoforms) was from Sigma-Aldrich. Guinea pig anti-SQSTM1 (p62-C) was from Progen. Anti-phospho-acetyl CoA carboxylase (Ser 79, #3661), anti-phospho-ribosomal RPS6 protein (Ser 240/244, #2215) and anti-LC3 (for immuno-cytochemistry, #2775) polyclonal rabbit antibodies are from Cell Signaling Technology. Mouse anti-WIPI2, rabbit anti-WIPI1 and rabbit anti-ATG13 were previously described.[7,28] Polyclonal rabbit anti-ULK1 antibody was generated against the peptide CSGRPGPFSSNRYGASV of the mouse ULK1 sequence and affinity-purifed using the SulfoLink immobilization kit for peptides (Pierce) according to the manufacturer's instructions. Alexa fluor 555 conjugated donkey anti-mouse antibody (A31570), Alexa fluor 488 conjugated donkey anti-rabbit antibody (A21206), and Alexa fluor 680 conjugated donkey anti-mouse antibody (A21057) were from Invitrogen. Dylight 800 conjugated goat anti-rabbit antibody (35571) was obtained from Thermoscientific. Donkey-anti-rabbit IgG conjugated to HRP (NA934V) and donkey-anti-mouse IgG conjugated to HRP (NA931V) were obtained from Sigma-Aldrich and rabbit-anti-guinea pig IgG conjugated to HRP (P0141) was from DakoCytomation.

ULK knockout mice. ULK1 targeted mice were derived from the AC0566 embryonic stem cell line (Wellcome Trust UK, Sanger Institute Gene Trap

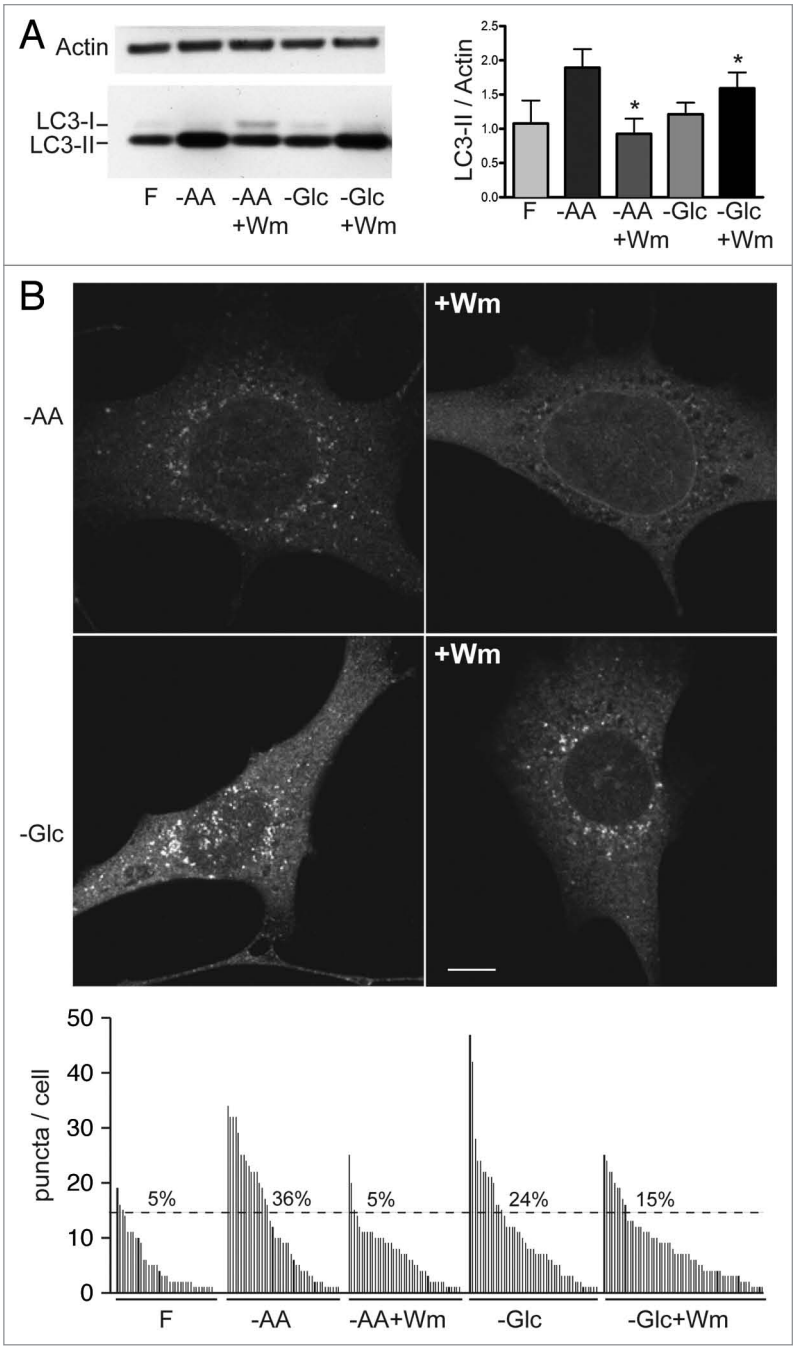

Figure 7. LC3 lipidation and autophagosome formation following glucose starvation are PtdIns3P-independent. (**A**) WT primary MEFs were treated with full-nutrient medium (F), EBSS (–AA), or EBSS containing 100 nM wortmannin (–AA+Wm) for 2 h. Alternatively, cells were incubated in glucose-free medium (–Glc) or glucose-free medium containing 100 nM wortmannin (–Glc+Wm) for 24 h. Resolved cells lysates were immunoblotted with antibodies for LC3 (Abcam polyclonal) and actin. Results are shown as average LC3-II/actin ± SEM (n = 4). Two-tailed paired t-tests were performed relative to equivalent treatment condition without wortmannin: *$p < 0.04$. (**B**) WT (immortalized) MEFs were treated with full-nutrient medium (F) or EBSS (–AA) for 2 h. Alternatively, cells were incubated in glucose-free medium (–Glc) for 16 h. Where indicated, incubations included 100 nM wortmannin (+Wm). Cells were fixed after treatments for LC3 immunostaining. Shown are representative confocal images of –AA and –Glc conditions ± wortmannin. Scale bar: 10 μm. Plot shows puncta/cell distributions for each condition. Each column represents quantification of one cell (40–60 cells/condition taken from two experiments). Shown are percentages of cells within each group containing 15 (or more) puncta/cell.

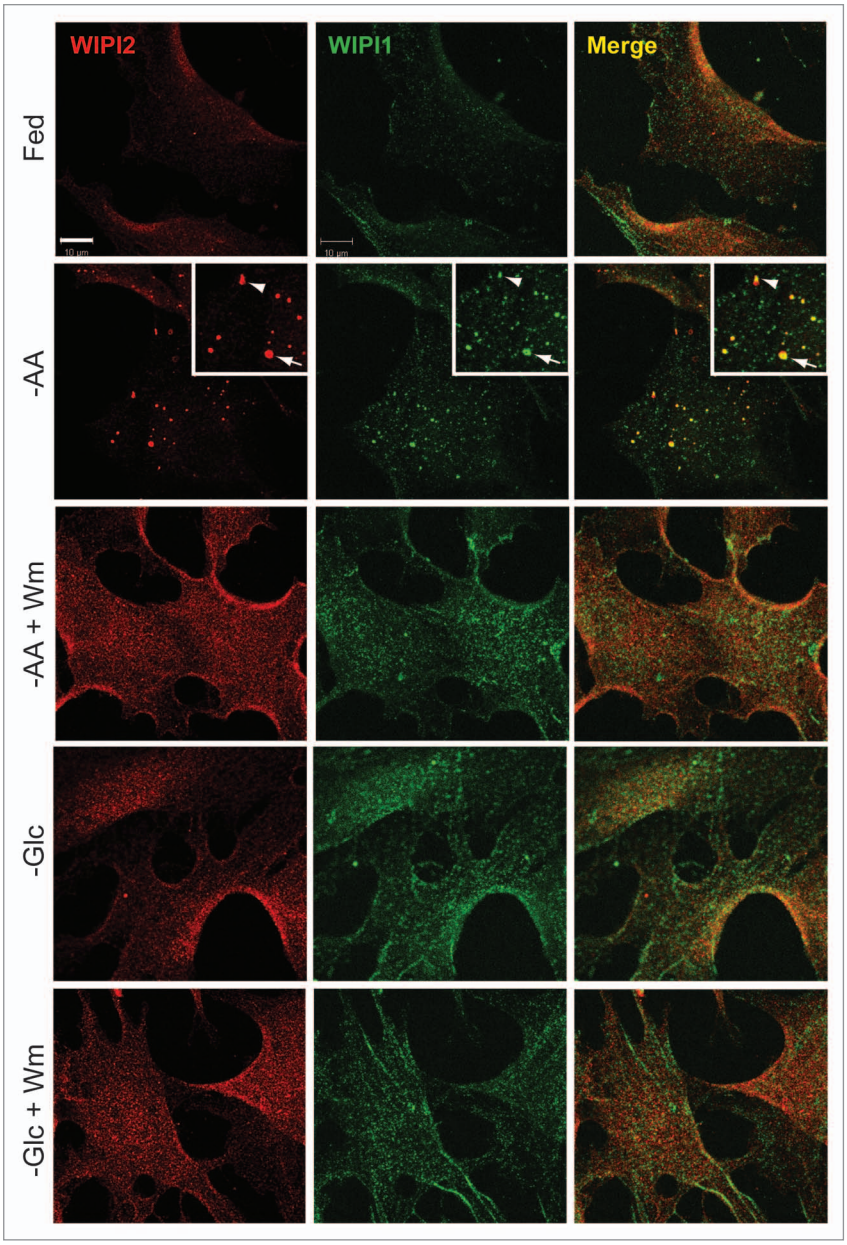

Figure 8. Absence of WIPI1- and WIPI2-positive autophagosomal membranes following glucose starvation. WT primary MEFs were incubated in full-nutrient medium (Fed), EBSS (–AA), or EBSS with 100 nM wortmannin (–AA+Wm) for 2 h. Alternatively, cells were glucose starved without or with 100 nM wortmannin (–Glc, –Glc+Wm) for 24 h before fixation. Cells were stained with antibodies against WIPI2 (red) and WIPI1 (green). Scale bar: 10 μm. Zoomed inset shows WIPI2 and WIPI1 colocalization following amino acid starvation (arrow: strong colocalization; arrowhead: partial).

Resource) that carries a pGT0lxr genetrap insertion within the 9.8 kb intron 3 to 4 of the mouse *Ulk1* locus. The pGT0lxr genetrap cassette contains the engrailed2 splice acceptor 5-prime to the β-geo selection marker (fusion of β-galactosidase/neomycin resistance). Location of genetrap insertion within intron 3 was mapped by PCR using ES cell-derived genomic DNA (further details in **Fig. S1**). A founder carrying germline transmission of *Ulk1* targeting was backcrossed onto the C57/Bl6 strain for 10 generations. *Ulk2* knockout mice were kindly provided by Dr. C. Tournier (University of Manchester, UK) and were previously described.[26] *Ulk1* knockout and *Ulk2* knockout mice were crossed to generate *Ulk1*/*Ulk2* double heterozygous mice. *Ulk1*/*Ulk2* double heterozygotes were intercrossed to produce the different genotypes characterized in this study. All animal work was performed in accordance with UK Home Office and Cancer Research UK institutional guidelines.

Generation and culture of mouse embryonic fibroblasts (MEFs). Pregnant female mice were sacrificed at 13.5 d past conception and the uterine horns removed. Separated embryos were decapitated and internal organs removed. Tissue was retained for genotyping. The remaining body tissue was minced finely then digested with 0.05% trypsin diluted in 0.2 g/L versene and 100 Kunitz units/mL of DNase I. Warm MEF medium (DMEM, 20% FBS, pen/strep and 4.8 mM L-glutamine) was added to the digested tissue, which was triturated briefly and remaining large tissue fragments allowed to settle. The supernatant containing cells was spun down at low speed and the resulting cell pellet from each embryo was resuspended in warm MEF medium and plated in a 10 cm tissue culture dish. After 24 h, unattached cells were discarded. MEFs were maintained in MEF medium. Stably replicating primary cultures derived through serial passage were used for experiments. MEFs were immortalized by transducing with retrovirus expressing SV40 T antigen from the pBabePuro vector. Experiments used either primary or immortalized lines as indicated in the legends. To generate MEFs stably expressing GFP ZFYVE1,[33] the coding portion of *GFP-Zfyve1* was subcloned into the pBabeHygro retroviral vector and virus stocks were used to transduce immortalized MEF lines followed by selection in hygromycin-containing media.

Genotyping. Tissue from the embryos used to produce the MEFs were digested with DirectPCR reagent (Viagen, 101-T) supplemented with 0.1 mg/mL proteinase K. PCR MegaMix-Blue (2MMB-5) was from Microzone, Ltd. PCR primers against *Ulk1* wild-type allele were F: 5'-ACT CGT GAG ATC TCA TGG CCA TGG-3' and R:5'-GCA TAA ATA GGA CCA AGT GGG CAC AGC-3'. Primers against genetrap cassette (*Ulk1* knockout allele) were F: 5'-ACA ACC AGG TCC CAG GTC CCG-3' and R: 5'-TTC AGG CTG CGC AAC TGT TGG-3'. Primers for the *Ulk2* alleles were previously reported.[26]

Transcript analysis. MEF cultures were lysed in Trizol reagent (Invitrogen Lifesciences) and total RNA was extracted according to the manufacturer's protocol. First strand cDNA was

synthesized from equal amounts of total RNA using oligo –dT primer and Bioscript reverse transcriptase (Bioline Reagents). Quantitative PCR was performed using the SensiMix SYBR (no-Rox) (Bioline Reagents) kit according to manufacturer's protocol. Real-time PCR primers: *Ulk1* forward TGC CCT TGA TGA GAT GTT CC, *Ulk1* reverse AGT CTC CTC TCA ATG CAC AGC; *Ulk2* forward TCG TTT ATC GCT ACC ACA AGG, *Ulk2* reverse GCC TGC TAC TCA CAC AGT TGC; β-*actin* forward GCC TTC CTT CTT GGG TAT GG, β-*actin* reverse GCA CTG TGT TGG CAT AGA GG .

Transfection of siRNAs. Knockdowns in MEFs were performed using siRNA directed against mouse Atg13 duplex 2 (Dharmacon, D-053540-02) and RISC-Free control siRNA (D-001220-01). Cells were treated with 20 nM siRNA and 0.25% Oligofectamine in OptiMEM for 6 h before replacement with MEF medium. siRNA transfections were repeated 24 h later. After a further 24 h, medium was refreshed and the cells were used for experiments 24 h later.

Amino acid and glucose starvation. For amino acid starvation, cells were rinsed and treated with either fresh MEF medium, EBSS or EBSS with bafilomycin A_1 for 2 h. For glucose starvation, cells were rinsed and treated with either fresh MEF medium, glucose-free MEF medium (glucose-free DMEM, dialyzed FBS, penicillin/streptomycin) or glucose-free MEF medium with bafilomycin A_1 for 16 to 24 h. Where indicated in legends, 100 nM wortmannin was added to glucose starvation samples 16 or 24 h before harvest. An additional 100 nM wortmannin was supplemented to these cultures 2 h before harvest, concurrent with the initiation of amino acid starvation treatments.

Immunoblotting. MEFS were washed with PBS and lysed in TNTE buffer (20 mM Tris pH 7.4, 150 mM NaCl, 5 mM EDTA, 1% TritonX-100) supplemented with complete protease inhibitor. Lysates were centrifuged and the post-nuclear supernatant was used for immunoblotting. Concentrated Laemmli buffer was added to the lysates and the samples were heated before being resolved on 4–12% gradient Bis-Tris acrylamide (NuPAGE) gels by electrophoresis using the MES buffer system. Proteins transferred onto PVDF membranes were blocked with 5% milk/TBS and incubated with anti-LC3, anti-actin, anti-ATG13, anti-ULK1 or anti-SQSTM1. Incubations with phospho-ACC and phospho-RPS6 primary antibodies were overnight in 5% BSA/TBS/0.1% Tween 20 as outlined in the manufacturer's protocol. Primary antibodies were detected using appropriate secondary antibodies and developed using standard enhanced chemiluminescence and film. Densitometry from film scans were quantitated using ImageJ software (NIH). Alternatively, LC3 (5F10), phospho-ACC, phospho-RPS6, and corresponding actin blots were visualized using the Odyssey (Li-Cor Biosciences) infrared quantitative imaging system.

Analysis of long-lived protein degradation. Long-lived protein degradation was performed as previously described.[48] Briefly, 35-mm dishes of WT, DKO#1, and DKO#2 MEFs were labeled for 24 h with 0.2 μCi C14-valine in DMEM containing 65 μM valine with 10% dialysed FCS. After 24 h the medium was replaced with full medium containing 2 mM valine. After an additional 24 h the cells were either washed and returned to full medium or incubated in EBSS for 2 h. Medium and cells were collected and the % long-lived protein degradation was calculated as described.[48]

Immunofluorescence. MEFs plated on glass coverslips were fixed for 20 min with 3% paraformaldehyde and permeabilized with ice-cold 100% methanol. Aldehyde autofluorescence was quenched with 50 mM NH_4Cl/PBS for 20 min. Cells were blocked with 5% BSA/PBS and incubated with mouse-anti-WIPI2 (1:400) or rabbit anti-WIPI1 (1:500) in 1% BSA/PBS. Cells were washed with PBS and incubated with Alexa fluor 555-conjugated donkey-anti-mouse IgG in 1% BSA/PBS. Images of WIPI1/2 were acquired on a Zeiss LSM 780 confocal microscope using a 40×/1.2NA objective and Zen 2010 software. For immunostaining of endogenous LC3, MEFs fixed in paraformaldehyde and methanol-permeabilized were blocked in gelatin/PBS before incubation with anti-LC3 (Cell Signaling) overnight. Primary staining was detected with anti-rabbit Alexa fluor 546. MEFs stably expressing GFP-ZFYVE1 were plated on glass coverslips, treated as indicated before fixation and visualization. Endogenous LC3 staining and GFP-ZFYVE1 fluorescence were captured on a Leica TCS SP5 confocal microscope fitted with a HCX PL APO CS-63x-1.4NA objective and a HyD GaAsP detection system (Leica Microsystems).

Quantification of puncta. WIPI2-positive spots were automatically counted using Imaris software (Bitplane). For each of two experiments, 10 fields were acquired per condition. Hoechst-stained nuclei were counted manually. Thresholds and spot sizes were set for each individual experiment. LC3 immunostaining was quantified using a custom image analysis macro designed in ImageJ that reported puncta and areas from images of single cells. Only puncta above a threshold size were used for analysis to exclude background. Images of GFP-ZFYVE1 puncta were manually scored by an observer that was unaware of sample identity. Data were compiled using Prism software (Graphpad). Statistical tests are detailed in the figure legends.

Disclosure of Potential Conflicts of Interest

No potential conflicts of interest were disclosed.

Acknowledgments

We thank Cathy Tournier for her generous gift of the *Ulk2*$^{-/-}$ mice. F.M. and S.A.T. are grateful to Cancer Research UK for funding. L. Williamson is grateful to the UK Biotechnology and Biological Sciences Research Council for support. E.Y.W.C. is grateful to the Royal Society of London for Improving Natural Knowledge for support. We thank Nicholas Ktistakis for the generous gift of the GFP-DFCP1 (ZFYVE1) plasmid and Noboru Mizushima for immortalized *Atg5*$^{-}$ knockout MEFs. We thank Nahoum Anthony for assistance on Perl programming used for image data analysis. F.M. and S.A.T. thank the members of the lab for helpful discussions and reading the manuscript.

Supplemental Materials

Supplemental materials may be found here:
www.landesbioscience.com/journals/autophagy/article/23066

References

1. Tooze SA, Jefferies HB, Kalie E, Longatti A, McAlpine FE, McKnight NC, et al. Trafficking and signaling in mammalian autophagy. IUBMB Life 2010; 62:503-8; PMID:20552641; http://dx.doi.org/10.1002/iub.334
2. Orsi A, Polson HE, Tooze SA. Membrane trafficking events that partake in autophagy. Curr Opin Cell Biol 2010; 22:150-6; PMID:20036114; http://dx.doi.org/10.1016/j.ceb.2009.11.013
3. Mizushima N, Yoshimori T, Ohsumi Y. The role of Atg proteins in autophagosome formation. Annu Rev Cell Dev Biol 2011; 27:107-32; PMID:21801009; http://dx.doi.org/10.1146/annurev-cellbio-092910-154005
4. Yan J, Kuroyanagi H, Kuroiwa A, Matsuda Y, Tokumitsu H, Tomoda T, et al. Identification of mouse ULK1, a novel protein kinase structurally related to C. elegans UNC-51. Biochem Biophys Res Commun 1998; 246:222-7; PMID:9600096; http://dx.doi.org/10.1006/bbrc.1998.8546
5. Kuroyanagi H, Yan J, Seki N, Yamanouchi Y, Suzuki Y, Takano T, et al. Human ULK1, a novel serine/threonine kinase related to UNC-51 kinase of Caenorhabditis elegans: cDNA cloning, expression, and chromosomal assignment. Genomics 1998; 51:76-85; PMID:9693035; http://dx.doi.org/10.1006/geno.1998.5340
6. Chan EY, Kir S, Tooze SA. siRNA screening of the kinome identifies ULK1 as a multidomain modulator of autophagy. J Biol Chem 2007; 282:25464-74; PMID:17595159; http://dx.doi.org/10.1074/jbc.M703663200
7. Chan EY, Longatti A, McKnight NC, Tooze SA. Kinase-inactivated ULK proteins inhibit autophagy via their conserved C-terminal domains using an Atg13-independent mechanism. Mol Cell Biol 2009; 29:157-71; PMID:18936157; http://dx.doi.org/10.1128/MCB.01082-08
8. Yan J, Kuroyanagi H, Tomemori T, Okazaki N, Asato K, Matsuda Y, et al. Mouse ULK2, a novel member of the UNC-51-like protein kinases: unique features of functional domains. Oncogene 1999; 18:5850-9; PMID:10557072; http://dx.doi.org/10.1038/sj.onc.1202988
9. Toda H, Mochizuki H, Flores R 3rd, Josowitz R, Krasieva TB, Lamorte VJ, et al. UNC-51/ATG1 kinase regulates axonal transport by mediating motor-cargo assembly. Genes Dev 2008; 22:3292-307; PMID:19056884; http://dx.doi.org/10.1101/gad.1734608
10. Zhou X, Babu JR, da Silva S, Shu Q, Graef IA, Oliver T, et al. Unc-51-like kinase 1/2-mediated endocytic processes regulate filopodia extension and branching of sensory axons. Proc Natl Acad Sci U S A 2007; 104:5842-7; PMID:17389358; http://dx.doi.org/10.1073/pnas.0701402104
11. Tomoda T, Kim JH, Zhan C, Hatten ME. Role of Unc51.1 and its binding partners in CNS axon outgrowth. Genes Dev 2004; 18:541-58; PMID:15014045; http://dx.doi.org/10.1101/gad.1151204
12. Hara T, Takamura A, Kishi C, Iemura S, Natsume T, Guan JL, et al. FIP200, a ULK-interacting protein, is required for autophagosome formation in mammalian cells. J Cell Biol 2008; 181:497-510; PMID:18443221; http://dx.doi.org/10.1083/jcb.200712064
13. Jung CH, Jun CB, Ro SH, Kim YM, Otto NM, Cao J, et al. ULK-Atg13-FIP200 complexes mediate mTOR signaling to the autophagy machinery. Mol Biol Cell 2009; 20:1992-2003; PMID:19225151; http://dx.doi.org/10.1091/mbc.E08-12-1249
14. Ganley IG, Lam H, Wang J, Ding X, Chen S, Jiang X. ULK1.ATG13.FIP200 complex mediates mTOR signaling and is essential for autophagy. J Biol Chem 2009; 284:12297-305; PMID:19258318; http://dx.doi.org/10.1074/jbc.M900573200
15. Hosokawa N, Hara T, Kaizuka T, Kishi C, Takamura A, Miura Y, et al. Nutrient-dependent mTORC1 association with the ULK1-Atg13-FIP200 complex required for autophagy. Mol Biol Cell 2009; 20:1981-91; PMID:19211835; http://dx.doi.org/10.1091/mbc.E08-12-1248
16. Hosokawa N, Sasaki T, Iemura S, Natsume T, Hara T, Mizushima N. Atg101, a novel mammalian autophagy protein interacting with Atg13. Autophagy 2009; 5:973-9; PMID:19597335; http://dx.doi.org/10.4161/auto.5.7.9296
17. Kraft C, Kijanska M, Kalie E, Siergiejuk E, Lee SS, Semplicio G, et al. Binding of the Atg1/ULK1 kinase to the ubiquitin-like protein Atg8 regulates autophagy. EMBO J 2012; 31:3691-703; PMID:22885598; http://dx.doi.org/10.1038/emboj.2012.225
18. Itakura E, Mizushima N. Characterization of autophagosome formation site by a hierarchical analysis of mammalian Atg proteins. Autophagy 2010; 6:764-76; PMID:20639694; http://dx.doi.org/10.4161/auto.6.6.12709
19. Bach M, Larance M, James DE, Ramm G. The serine/threonine kinase ULK1 is a target of multiple phosphorylation events. Biochem J 2011; 440:283-91; PMID:21819378; http://dx.doi.org/10.1042/BJ20101894
20. Egan D, Kim J, Shaw RJ, Guan KL. The autophagy initiating kinase ULK1 is regulated via opposing phosphorylation by AMPK and mTOR. Autophagy 2011; 7:643-4; PMID:21460621; http://dx.doi.org/10.4161/auto.7.6.15123
21. Kim J, Kundu M, Viollet B, Guan KL. AMPK and mTOR regulate autophagy through direct phosphorylation of Ulk1. Nat Cell Biol 2011; 13:132-41; PMID:21258367; http://dx.doi.org/10.1038/ncb2152
22. Shang L, Chen S, Du F, Li S, Zhao L, Wang X. Nutrient starvation elicits an acute autophagic response mediated by Ulk1 dephosphorylation and its subsequent dissociation from AMPK. Proc Natl Acad Sci U S A 2011; 108:4788-93; PMID:21383122; http://dx.doi.org/10.1073/pnas.1100844108
23. Jung CH, Seo M, Otto NM, Kim DH. ULK1 inhibits the kinase activity of mTORC1 and cell proliferation. Autophagy 2011; 7:1212-21; PMID:21795849; http://dx.doi.org/10.4161/auto.7.10.16660
24. Lin SY, Li TY, Liu Q, Zhang C, Li X, Chen Y, et al. GSK3-TIP60-ULK1 signaling pathway links growth factor deprivation to autophagy. Science 2012; 336:477-81; PMID:22539723; http://dx.doi.org/10.1126/science.1217032
25. Kundu M, Lindsten T, Yang CY, Wu J, Zhao F, Zhang J, et al. Ulk1 plays a critical role in the autophagic clearance of mitochondria and ribosomes during reticulocyte maturation. Blood 2008; 112:1493-502; PMID:18539900; http://dx.doi.org/10.1182/blood-2008-02-137398
26. Lee EJ, Tournier C. The requirement of uncoordinated 51-like kinase 1 (ULK1) and ULK2 in the regulation of autophagy. Autophagy 2011; 7:689-95; PMID:21460635; http://dx.doi.org/10.4161/auto.7.7.15450
27. Egan DF, Shackelford DB, Mihaylova MM, Gelino S, Kohnz RA, Mair W, et al. Phosphorylation of ULK1 (hATG1) by AMP-activated protein kinase connects energy sensing to mitophagy. Science 2011; 331:456-61; PMID:21205641; http://dx.doi.org/10.1126/science.1196371
28. Polson HE, de Lartigue J, Rigden DJ, Reedijk M, Urbé S, Clague MJ, et al. Mammalian Atg18 (WIPI2) localizes to omegasome-anchored phagophores and positively regulates LC3 lipidation. Autophagy 2010; 6:506-22; PMID:20505359; http://dx.doi.org/10.4161/auto.6.4.11863
29. Blommaart EF, Krause U, Schellens JP, Vreeling-Sindelárová H, Meijer AJ. The phosphatidylinositol 3-kinase inhibitors wortmannin and LY294002 inhibit autophagy in isolated rat hepatocytes. Eur J Biochem 1997; 243:240-6; PMID:9030745; http://dx.doi.org/10.1111/j.1432-1033.1997.0240a.x
30. Kuma A, Hatano M, Matsui M, Yamamoto A, Nakaya H, Yoshimori T, et al. The role of autophagy during the early neonatal starvation period. Nature 2004; 432:1032-6; PMID:15525940; http://dx.doi.org/10.1038/nature03029
31. Komatsu M, Waguri S, Ueno T, Iwata J, Murata S, Tanida I, et al. Impairment of starvation-induced and constitutive autophagy in Atg7-deficient mice. J Cell Biol 2005; 169:425-34; PMID:15866887; http://dx.doi.org/10.1083/jcb.200412022
32. Saitoh T, Fujita N, Hayashi T, Takahara K, Satoh T, Lee H, et al. Atg9a controls dsDNA-driven dynamic translocation of STING and the innate immune response. Proc Natl Acad Sci U S A 2009; 106:20842-6; PMID:19926846; http://dx.doi.org/10.1073/pnas.0911267106
33. Axe EL, Walker SA, Manifava M, Chandra P, Roderick HL, Habermann A, et al. Autophagosome formation from membrane compartments enriched in phosphatidylinositol 3-phosphate and dynamically connected to the endoplasmic reticulum. J Cell Biol 2008; 182:685-701; PMID:18725538; http://dx.doi.org/10.1083/jcb.200803137
34. Cheong H, Lindsten T, Wu J, Lu C, Thompson CB. Ammonia-induced autophagy is independent of ULK1/ULK2 kinases. Proc Natl Acad Sci U S A 2011; 108:11121-6; PMID:21690395; http://dx.doi.org/10.1073/pnas.1107969108
35. Codogno P, Mehrpour M, Proikas-Cezanne T. Canonical and non-canonical autophagy: variations on a common theme of self-eating? Nat Rev Mol Cell Biol 2012; 13:7-12; PMID:22166994
36. Proikas-Cezanne T, Ruckerbauer S, Stierhof YD, Berg C, Nordheim A. Human WIPI-1 puncta-formation: a novel assay to assess mammalian autophagy. FEBS Lett 2007; 581:3396-404; PMID:17618624; http://dx.doi.org/10.1016/j.febslet.2007.06.040
37. Tsukada M, Ohsumi Y. Isolation and characterization of autophagy-defective mutants of Saccharomyces cerevisiae. FEBS Lett 1993; 333:169-74; PMID:8224160; http://dx.doi.org/10.1016/0014-5793(93)80398-E
38. Chan EY. Regulation and function of uncoordinated-51 like kinase proteins. Antioxid Redox Signal 2012; 17:775-85; PMID:22074133; http://dx.doi.org/10.1089/ars.2011.4396
39. Chan EY, Tooze SA. Evolution of Atg1 function and regulation. Autophagy 2009; 5:758-65; PMID:19411825.
40. Young AR, Narita M, Ferreira M, Kirschner K, Sadaie M, Darot JF, et al. Autophagy mediates the mitotic senescence transition. Genes Dev 2009; 23:798-803; PMID:19279323; http://dx.doi.org/10.1101/gad.519709
41. Alers S, Löffler AS, Paasch F, Dieterle AM, Keppeler H, Lauber K, et al. Atg13 and FIP200 act independently of Ulk1 and Ulk2 in autophagy induction. Autophagy 2011; 7:1423-33; PMID:22024743; http://dx.doi.org/10.4161/auto.7.12.18027
42. Itakura E, Kishi C, Inoue K, Mizushima N. Beclin 1 forms two distinct phosphatidylinositol 3-kinase complexes with mammalian Atg14 and UVRAG. Mol Biol Cell 2008; 19:5360-72; PMID:18843052; http://dx.doi.org/10.1091/mbc.E08-01-0080
43. Matsunaga K, Morita E, Saitoh T, Akira S, Ktistakis NT, Izumi T, et al. Autophagy requires endoplasmic reticulum targeting of the PI3-kinase complex via Atg14L. J Cell Biol 2010; 190:511-21; PMID:20713597; http://dx.doi.org/10.1083/jcb.200911141
44. Pfisterer SG, Mauthe M, Codogno P, Proikas-Cezanne T. Ca2+/calmodulin-dependent kinase (CaMK) signaling via CaMKI and AMP-activated protein kinase contributes to the regulation of WIPI-1 at the onset of autophagy. Mol Pharmacol 2011; 80:1066-75; PMID:21896713; http://dx.doi.org/10.1124/mol.111.071761
45. Nishida Y, Arakawa S, Fujitani K, Yamaguchi H, Mizuta T, Kanaseki T, et al. Discovery of Atg5/Atg7-independent alternative macroautophagy. Nature 2009; 461:654-8; PMID:19794493; http://dx.doi.org/10.1038/nature08455

46. Scarlatti F, Maffei R, Beau I, Codogno P, Ghidoni R. Role of non-canonical Beclin 1-independent autophagy in cell death induced by resveratrol in human breast cancer cells. Cell Death Differ 2008; 15:1318-29; PMID:18421301; http://dx.doi.org/10.1038/cdd.2008.51

47. Mauthe M, Jacob A, Freiberger S, Hentschel K, Stierhof Y-D, Codogno P, et al. Resveratrol-mediated autophagy requires WIPI-1-regulated LC3 lipidation in the absence of induced phagophore formation. Autophagy 2011; 7:1448-61; PMID:22082875; http://dx.doi.org/10.4161/auto.7.12.17802

48. Köchl R, Hu XW, Chan EY, Tooze SA. Microtubules facilitate autophagosome formation and fusion of autophagosomes with endosomes. Traffic 2006; 7:129-45; PMID:16420522; http://dx.doi.org/10.1111/j.1600-0854.2005.00368.x